Promoting magnetic dipolar transition in trivalent lanthanide ions with lossless Mie resonances

Brice Rolly,[1] Betina Bebey,[1] Sebastien Bidault,[2] Brian Stout,[1] and Nicolas Bonod[1,*]

[1]*Institut Fresnel, CNRS, Aix-Marseille Université, Ecole Centrale Marseille Campus de Saint-Jérôme, 13013 Marseille, France*

[2]*Institut Langevin, ESPCI ParisTech, CNRS, 1 rue Jussieu, 75005 Paris, France*

(Received 24 January 2012; revised manuscript received 4 May 2012; published 18 June 2012)

Mie resonances in dielectric particles can increase the local optical density of states (LDOS) associated with either electric or magnetic transition rates in nearby quantum emitters without ohmic losses. Their rather large quality factors compensate their low field confinement as compared to the plasmon resonances of metallic nanostructures for which nonradiative decay channels dominate. We show theoretically that near-infrared quadrupolar magnetic resonances in silicon particles can preferentially promote magnetic versus electric radiative deexcitation in trivalent erbium ions at 1.54 μm. The distance dependent interaction between magnetic (electric) dipole emitters and induced magnetic or electric dipoles and quadrupoles is derived analytically and compared to quasiexact full-field calculations based on Mie theory. We discuss how near-field coupling between nearby particles can further enhance the magnetic LDOS and compensate for the weak refractive index contrasts between dielectric particles and a typical host matrix for the lanthanide ions.

DOI: 10.1103/PhysRevB.85.245432 PACS number(s): 32.50.+d, 32.70.−n, 78.67.−n

I. INTRODUCTION

Since the pioneering work of Purcell, it has been established that decay rates are not intrinsic properties of quantum emitters, and that they strongly depend on the local electromagnetic environment.[1–3] The magnetic dipole transition of quantum emitters is in most cases five orders of magnitude smaller than electric dipole transitions, thereby explaining why magnetic effects are typically ignored in light-matter interactions. Studies on the enhancement of transition rates in solid-state systems consequently focused on coupling emitters to photonic cavities with high quality factors or to metallic nanoscale resonators. In the latter case, nanogap metallic antennas supporting lossy plasmon polaritons feature broad resonances whose low quality factors are compensated by high field confinement,[4–6] making them one of the most widely studied plasmonic devices for enhancing the electric dipolar decay rates of quantum emitters at room temperature.[7]

Concurrently, the development of metamaterials has shown that, by engineering metallic nanostructures, it is possible to artificially increase the magnetic response of matter and design left-handed metamaterials[8] or map the magnetic fields in near-field optical microscopy.[9,10] Furthermore, quantum emitters with forbidden dipole transitions like trivalent lanthanide ions[11,12] undergo magnetic spontaneous emission. In such systems, magnetic and electric dipole transitions are competitive decay channels from a common excited state. Karaveli and Zia recently demonstrated that, in the vicinity of a gold mirror, the LDOS corresponding to electric and magnetic transitions is maximum at different positions and can promote magnetic emission from europium ions.[13,14] Feng *et al.* proposed to increase magnetic emission while quenching electric emission by using a plasmon resonance in a metallic slab having a large induced magnetic dipole.[15] Unfortunately, metallic nanostructures exhibit nonradiative decay channels for both magnetic and electric transition dipoles. Consequently, even when radiative electric transition rates are low, magnetic emission can still be quenched by nonradiative electric decay channels.

Magnetic resonances in dielectric particles are thus an attractive alternative to promote magnetic emission in quantum emitters without introducing nonradiative decay channels. Compared to plasmon polaritons, they feature higher quality factors thanks to their low radiative and ohmic dampings[16] which compensate their weaker field confinement. Furthermore, their frequency widths remain larger than the homogeneous linewidths of trivalent lanthanide ions at room temperature. In particular, the quadrupolar magnetic resonance of a single silicon particle can be used to promote the magnetic component of the ${}^4I_{13/2} \rightarrow {}^4I_{15/2}$ transition around $\lambda = 1540$ nm in Er^{3+} ions. In typical host matrices, the relative strength of magnetic versus electric emission for this transition is 10–40% depending on the local crystal-field symmetry.[11,12] More generally, we derive analytical expressions of the radiative and total decay rates for electric and magnetic transition dipoles in the vicinity of spheres exhibiting dipolar and quadrupolar, electric and magnetic resonances.

II. ENHANCING THE MAGNETIC DIPOLAR TRANSITION WITH QUADRUPOLAR MIE RESONANCE

We compute the decay rates for electric and magnetic dipole emitters placed close to a dielectric sphere made of silicon (refractive index function taken from Palik[17]) by calculating the imaginary part of the dyadic Green's function in a generalized multiple particle Mie formalism (GMM).[18] We at first consider a surrounding medium made of air ($n = 1$ refractive index host medium). Since the imaginary part of the dielectric constant of silicon for the considered range of near-infrared frequencies is negligible, the radiative and total decay rates are equal. The diameter of the sphere $2a = 615$ nm is chosen in order to optimize the decay rates of the magnetic dipole transition near $\lambda = 1540$ nm using a quadrupolar magnetic Mie resonance. The results displayed in Fig. 1 show that a single dielectric sphere significantly enhances the normalized decay rates $\tilde{\Gamma} = \Gamma/\Gamma_0$ of a magnetic dipole emitter. The maximum decay rate enhancements occur with longitudinal couplings and can reach two orders of

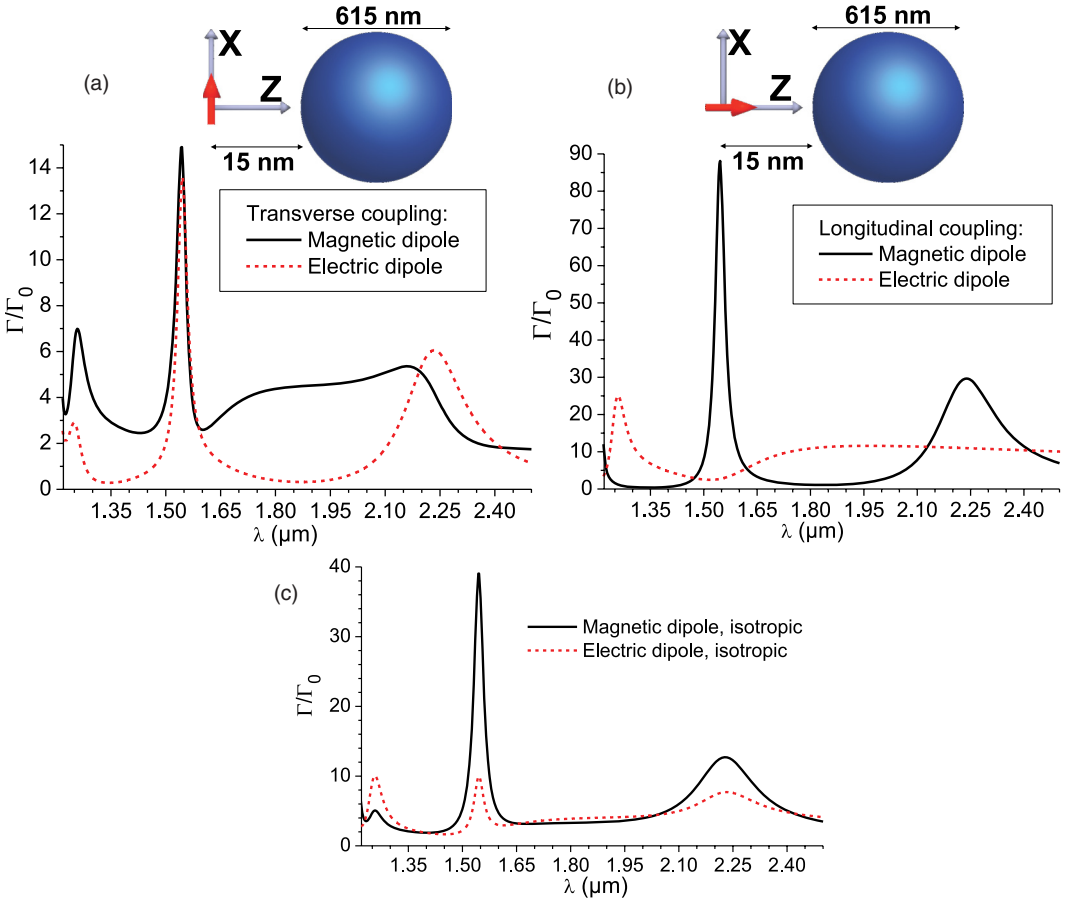

FIG. 1. (Color online) Normalized decay rates, Γ/Γ_0, as a function of the wavelength, for an emitter placed at 15 nm from the surface of a Si sphere of diameter $2a = 615$ nm. The surrounding medium is air. Full black line: magnetic dipole emitter; dashed red line: electric dipole emitter. (a) Transverse coupling, (b) longitudinal coupling and (c) isotropic average over dipole orientations. Insets: sketch of the emitter coupled to the dielectric particle. The dipole moment is represented by a red arrow.

magnitude (e.g., at $\lambda = 1546$ nm) for a magnetic dipole emitter whereas it is limited to 25 for an electric transition dipole. For a longitudinal coupling, the magnetic and electric transitions have decay rate enhancement factors that are spectrally well separated, whereas for a transverse coupling, both electric and magnetic emitters exhibit common maxima. The isotropic orientation average over the dipolar moment ($\tilde{\Gamma}_{\text{iso}} = 2/3\tilde{\Gamma}_{||} + 1/3\tilde{\Gamma}_{\perp}$, where $||$ and $\perp$ stand for transverse and longitudinal couplings respectively) is plotted in Fig. 1(c) with respect to the wavelength and confirms that the magnetic deexcitation is promoted by coupling the emitter to the magnetic quadrupole resonance of the dielectric resonator. The magnetic decay rate enhancement reaches 40 near $\lambda = 1540$ nm and is four times higher than the electric decay rates.

In order to analyze the relative influence of the different Mie resonances in the decay rate maxima, we display in Fig. 2 the decay rates reported in Fig. 1(a) for transverse illumination by a magnetic dipole, together with the amplitudes of the electric and magnetic dipole and quadrupole Mie coefficients. The four maxima of the decay rates are thus due to the excitation of both electric and magnetic resonances (dipolar and quadrupolar) with the highest decay rate enhancements offered by the magnetic quadrupole resonance. Cross-coupling between magnetic dipolar emitters and electric Mie resonances (and vice versa) only occurs in transverse coupling, thus explaining why in Fig. 1(a) the electric and magnetic decay rates both present a maximum at the same wavelength ($\lambda = 1544$ nm). For a longitudinal coupling [Fig. 1(b)], the decay rates corresponding to electric or magnetic transitions are only

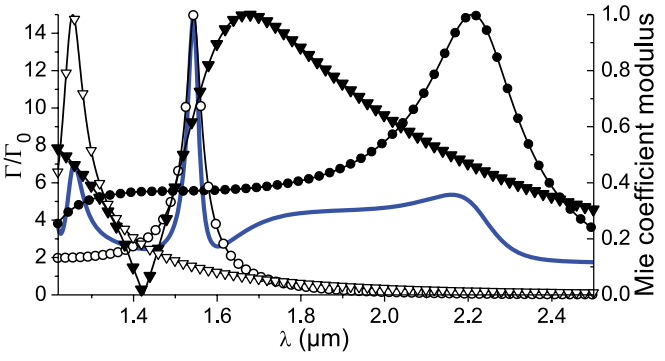

FIG. 2. (Color online) (Left scale, thick blue line) Decay rates for a magnetic dipole transversely coupled to a $2a = 615$ nm diameter sphere as a function of the wavelength. (Right scale) Modulus of the Mie coefficients of the sphere: (full circles) magnetic dipole, b_1; (full triangles) electric dipole, a_1; (open circles) magnetic quadrupole, b_2; (open triangles) electric quadrupole, a_2.

enhanced when coupled to multipolar Mie resonances of the same electromagnetic nature.

Multipolar resonances have not been considered for the enhancement of radiative decay rates using metallic nanoantennas on account of their high losses and inability to efficiently radiate in the far-field. The situation is different for dielectrics: negligible ohmic losses mean that the electromagnetic energy emitted by the dipolar source can be stored in multipolar Mie resonances with higher quality factors before being fully radiated in the far-field. The drawback is a selective spectral window [e.g., approx. 30 nm full width half maximum (FWHM) for the magnetic quadrupole resonance in the longitudinal case here] which would be inadequate for the homogeneously broadened fluorescence spectra of organic dyes at room temperature, but matches the narrow emission bands of lanthanide ions such as trivalent erbium at 1540 nm.

III. ANALYTICAL EXPRESSIONS OF THE DIPOLAR AND QUADRUPOLAR DECAY RATES

To fully describe the cross-coupling between electric and magnetic responses in the calculated decay rates, we now derive analytical expressions for the total and radiative decay rates in transverse and longitudinal coupling for the first two electric and magnetic Mie resonances. For this purpose, we use matricial expressions of the radiative and total decay rates of an emitter placed in the vicinity of an ensemble of spheres. When considering only one particle, they take the form:

$$\tilde{\Gamma}_{\text{tot}} = 1 + 6\pi \text{Re}[f^\dagger H^{(\text{em,s})} t H^{(\text{s,em})} f], \tag{1}$$

$$\begin{aligned}\tilde{\Gamma}_{\text{rad}} &= 1 + 6\pi [f^\dagger H^{(\text{s,em})\dagger} t^\dagger t H^{(\text{s,em})} f] \\ &\quad + 12\pi \text{Re}(f^\dagger J^{(\text{em,s})} t H^{(\text{s,em})} f),\end{aligned} \tag{2}$$

where f is a column matrix containing the excitation coefficients, H is an irregular translation matrix between the emitter (em) and the sphere (s), J is a regular translation matrix, and t is a diagonal matrix composed of the Mie coefficients of the sphere.[18] We consider a single particle sphere placed in the $+z$ direction with respect to a dipole emitter oriented either transversally ("orbital" number $m = 1$, dipole moment oriented on the x axis) or longitudinally ($m = 0$, dipole moment oriented on the z axis). With a quadrupolar assumption, they can be cast:

$$f = \begin{bmatrix} e_1 \\ 0 \\ h_1 \\ 0 \end{bmatrix}, \quad H^{(\text{em,s})} = \begin{bmatrix} A(kd) & B(kd) \\ B(kd) & A(kd) \end{bmatrix},$$

$$J^{(\text{em,s})} = \begin{bmatrix} C(kd) & D(kd) \\ D(kd) & C(kd) \end{bmatrix}, \quad t = \text{Diag}\left(c_1^e, c_2^e, c_1^m, c_2^m\right).$$

The superscripts (s,em) and (em,s) respectively refer to a translation from the emitter to the sphere, and from the sphere to the emitter. The coefficients h_1 (null for an electric emitter) and e_1 (null for a magnetic emitter) are the incident magnetic and electric dipole coefficients, normalized to $1/\sqrt{6\pi}$. The Mie coefficients correspond to the polarizabilities via the relation $\alpha_j^{e,m} = \frac{6\pi}{ik^3} c_j^{e,m}$.[18] The two coupling geometries will involve $A_{n,m,\nu,\mu}$ and $B_{n,m,\nu,\mu}$ matrix blocks, where $[A|B]_{n,m,\nu,\mu}$ is the coupling from the multipole order n with orbital number m, to the multipole order ν with orbital number μ:

$$\begin{aligned} A^{\text{L}}(kd) &= \begin{bmatrix} A_{1,0,1,0} & A_{1,0,2,0} \\ A_{1,0,2,0} & A_{2,0,2,0} \end{bmatrix}, \\ A^{\text{T}}(kd) &= \begin{bmatrix} A_{1,1,1,1} & A_{1,1,2,1} \\ A_{1,1,2,1} & A_{2,1,2,1} \end{bmatrix}, \\ B^{\text{L}}(kd) &= 0, \\ B^{\text{T}}(kd) &= \begin{bmatrix} B_{1,1,1,1} & B_{1,1,2,1} \\ B_{1,1,2,1} & B_{2,1,2,1} \end{bmatrix}. \end{aligned}$$

The C and D blocks feature the same symmetries as the A and B blocks respectively. The L and T superscripts refer respectively to longitudinal or transverse couplings. When computing $H^{(\text{s,em})}$, we obtain the simple relation:

$$H^{(s,\text{em})} = \begin{bmatrix} A & -B \\ -B & A \end{bmatrix}. \tag{3}$$

The right-hand side of Eqs. (1) and (2) can thus be cast:

$$\tilde{\Gamma}_{\text{tot}}^{\text{L,u}} = 1 + \text{Re}\left[c_1^u (A_{1,0,1,0})^2 + c_2^u (A_{1,0,2,0})^2\right], \tag{4}$$

$$\begin{aligned}\tilde{\Gamma}_{\text{tot}}^{\text{T,u}} &= 1 + \text{Re}\left[c_1^u (A_{1,1,1,1})^2 + c_2^u (A_{1,1,2,1})^2\right. \\ &\quad \left. - c_1^v (B_{1,1,1,1})^2 - c_2^v (B_{1,1,2,1})^2\right],\end{aligned} \tag{5}$$

$$\begin{aligned}\tilde{\Gamma}_{\text{rad}}^{\text{L,u}} &= 1 + \left|c_1^u A_{1,0,1,0}\right|^2 + \left|c_2^u A_{1,0,2,0}\right|^2 \\ &\quad + 2\text{Re}\left(c_1^u A_{1,0,1,0} C_{1,0,1,0} + c_2^u A_{1,0,2,0} C_{1,0,2,0}\right),\end{aligned} \tag{6}$$

$$\begin{aligned}\tilde{\Gamma}_{\text{rad}}^{\text{T,u}} &= 1 + \left|c_1^u A_{1,1,1,1}\right|^2 + \left|c_2^u A_{1,1,2,1}\right|^2 \\ &\quad + \left|c_1^v B_{1,1,1,1}\right|^2 + \left|c_2^v B_{1,1,2,1}\right|^2 \\ &\quad + 2\text{Re}\left(c_1^u A_{1,1,1,1} C_{1,1,1,1} + c_2^u A_{1,1,2,1} C_{1,1,2,1}\right. \\ &\quad \left. - c_1^v B_{1,1,1,1} D_{1,1,1,1} - c_2^v B_{1,1,2,1} D_{1,1,2,1}\right),\end{aligned} \tag{7}$$

where u and v refer to electric ($u = e$, $v = m$) or magnetic ($u = m$, $v = e$) emitters. The A and B coefficients can be calculated from Ref. 19 with the angles $\theta = \phi = 0$:

$$\begin{aligned} A_{1,1,1,1} &= \frac{1}{2}\left(\bar{\alpha}_{1,1,1,1}^s + \bar{\alpha}_{1,0,1,0}^s\right) \\ &= \frac{1}{2}\left(\bar{\alpha}_{0,0,0,0}^s + \frac{b_{2,0}^-}{b_{0,0}^+}\bar{\alpha}_{2,0,0,0}^s + \bar{\alpha}_{0,0,0,0}^s + \frac{a_{2,0}^-}{a_{0,0}^+}\bar{\alpha}_{2,0,0,0}^s\right) \\ &= \frac{1}{2}\left(\frac{-1}{\sqrt{5}}\bar{\alpha}_{2,0,0,0}^s + 2\bar{\alpha}_{0,0,0,0}^s\right) \\ &= -\frac{1}{2\sqrt{5}}\sqrt{4\pi}\,Y_{2,0}(0,0)h_2(kd) + \sqrt{4\pi}\,Y_{0,0}(0,0)h_0(kd) \\ &= -\frac{P_2^0(1)}{2}h_2(kd) + P_0^0(1)h_0(kd) \\ &= \frac{1}{2}[2h_0(kd) - h_2(kd)] \\ A_{1,1,1,1} &= \frac{3i}{2}\frac{e^{ikd}}{(kd)^3}[1 - ikd - (kd)^2]. \end{aligned}$$

Similarly, the other coefficients can be cast:

$$B_{1,1,1,1} = \frac{3i}{2}\frac{e^{ikd}}{(kd)^2}(kd + i), \quad A_{1,0,1,0} = -3i\frac{e^{ikd}}{(kd)^3}(1 - ikd),$$

$$A_{1,0,2,0} = \frac{3}{\sqrt{5}}\frac{e^{ikd}}{(kd)^4}[5i(kd)^2 - 15kd - 15i],$$

$$A_{1,1,2,1} = \frac{\sqrt{15}}{2}\frac{e^{ikd}}{(kd)^4}[-(kd)^3 - 3i(kd)^2 + 6kd + 6i],$$

$$B_{1,1,2,1} = \frac{\sqrt{15}}{2}\frac{e^{ikd}}{(kd)^3}[-(kd)^2 - 3ikd + 3].$$

The C and D coefficients are calculated with the same expressions except that the spherical Hankel functions are replaced by the spherical Bessel functions j_n:

$$C_{1,1,1,1} = \mathrm{Re}(A_{1,1,1,1}), \quad C_{1,0,1,0} = \mathrm{Re}(A_{1,0,1,0}),$$
$$C_{1,0,2,0} = \mathrm{Re}(A_{1,0,2,0}), \quad D_{1,1,1,1} = i\,\mathrm{Im}(B_{1,1,1,1}),$$
$$D_{1,1,2,1} = i\,\mathrm{Im}(B_{1,1,2,1}).$$

In the case of lossless materials, expressions of $\tilde{\Gamma}_{\mathrm{rad}}$ and $\tilde{\Gamma}_{\mathrm{tot}}$ give the same results due to energy conservation, and we will only refer in the following to the formulations of $\tilde{\Gamma}_{\mathrm{tot}}$.

The $\mathrm{Re}(c_i^u A_{1,x,i,x}^2)$ term corresponds to the decay rate enhancement produced by the magnetic (respectively electric) dipolar ($i = 1$) or quadrupolar ($i = 2$) Mie resonances of the sphere for a magnetic (respectively electric) dipolar emitter. This term appears in both longitudinal and transverse coupling cases. On the other hand, the $\mathrm{Re}(c_i^v B_{1,1,i,1}^2)$ term describes the level of cross-coupling between an electric dipole emitter and a magnetic ith order multipole resonance (and vice versa), and only arises for transverse coupling. Let us emphasize that this coupling only occurs for an emitter component perpendicular to the emitter-sphere axis, since the magnetic field from an electric dipole (respectively the electric field from a magnetic dipole) is null along the dipole axis. The analytical expressions of the four contributions to the normalized total decay rate in transverse coupling can then be derived. The coupling between an emitting dipole and a dipolar resonance of the same type can be cast as

$$1 + \mathrm{Re}\left(c_1^u A_{1,1,1,1}^2\right) = 1 + \frac{3k^3}{8\pi}\mathrm{Im}\left[\frac{\alpha_1^u e^{2ikd}}{(kd)^6}(1 - 2ikd - 3k^2d^2 + 2ik^3d^3 + k^4d^4)\right], \quad (8)$$

with $u = m$ for a magnetic dipole or $u = e$ for an electric dipole. In the latter case, we recognize the expression derived by Carminati *et al.* for an electric dipolar approximation.[6] The coupling between the emitter and the quadrupolar resonance of the same type, on the other hand, modifies the total decay rate via the term

$$1 + \mathrm{Re}\left(c_1^u A_{1,1,2,1}^2\right) = 1 - \frac{5k^3}{8\pi}\mathrm{Im}\left[\frac{\alpha_2^u e^{2ikd}}{(kd)^8}(-k^3d^3 - 3ik^2d^2 + 6kd + 6i)^2\right]. \quad (9)$$

The cross-coupling terms for both the induced dipole and quadrupole can be cast:

$$1 - \mathrm{Re}\left(c_1^v B_{1,1,1,1}^2\right) = 1 - \frac{3k^3}{8\pi}\mathrm{Im}\left[\frac{\alpha_1^v e^{2ikd}}{(kd)^4}(kd+i)^2\right], \quad (10)$$

$$1 - \mathrm{Re}\left(c_2^v B_{1,1,2,1}^2\right) = 1 + \frac{5k^3}{8\pi}\mathrm{Im}\left[\frac{\alpha_2^v e^{2ikd}}{(kd)^6}(3 - 3ikd - k^2d^2)^2\right], \quad (11)$$

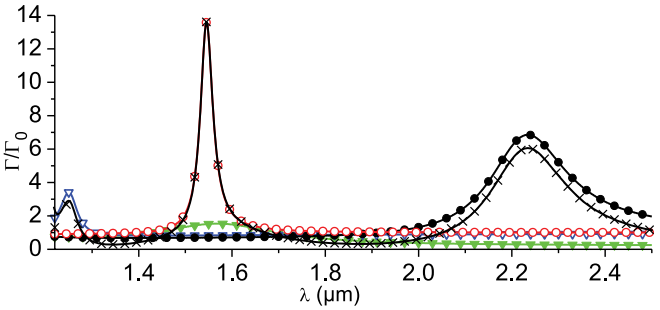

FIG. 3. (Color online) (Black line) Normalized radiative decay rate of an electric dipole transversely coupled to a Si sphere, (crosses) sum of the right-hand sides of Eqs. (8)–(11). Contributions from the different induced multipoles: (full black circles) magnetic dipole, (full green triangles) electric dipole, (open red circles) magnetic quadrupole, (open blue triangles) electric quadrupole. A value below 1 means that the corresponding multipole lowers the decay rate.

respectively. For a longitudinal coupling, the cross-coupling terms are null and the total decay rates are linked to the coupling between an emitter and a dipolar and quadrupolar resonance of the same type which can be expressed respectively as:

$$1 + \mathrm{Re}\left(c_1^u A_{1,0,1,0}^2\right) = 1 + \frac{3k^3}{2\pi}\mathrm{Im}\left[\frac{\alpha_1^u e^{2ikd}}{(kd)^6}(1 - ikd)^2\right] \quad (12)$$

$$1 + \mathrm{Re}\left(c_1^u A_{1,0,2,0}^2\right) = 1 - \frac{3k^3}{10\pi}\mathrm{Im}\left[\frac{\alpha_2^u e^{2ikd}}{(kd)^8}(-25[kd]^2 - 15kd - 15i)^2\right]. \quad (13)$$

We plot in Fig. 3 the right-hand sides of Eqs. (8)–(11) obtained when an electric dipole is transversely coupled with a dielectric sphere ($u = e$ and $v = m$). Let us remark that the sum of the right-hand sides of the four expressions is then equal to $\tilde{\Gamma}_{\mathrm{rad}}^{\mathrm{T,e}} + 3$. We see in Fig. 3 that this sum minus 3 (crosses) corresponds

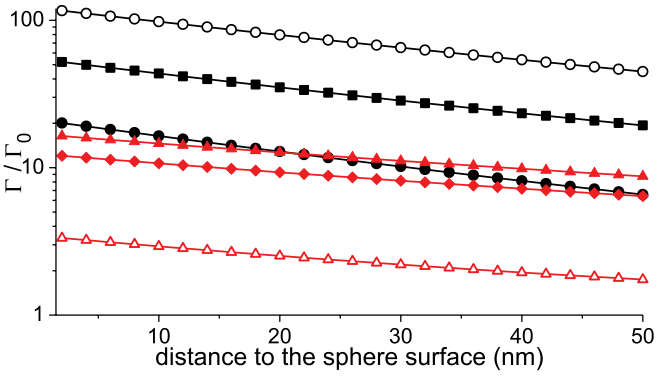

FIG. 4. (Color online) Normalized decay rates with respect to the distance between the emitter and the surface of the particle, wavelength $\lambda = 1546$ nm. Same parameters as in Fig. 1. (Black circles) magnetic dipoles, (red triangles) electric dipoles, full symbols: transverse coupling, open symbols: longitudinal coupling. Isotropic averages : (black squares) magnetic dipole, (red diamonds) electric dipole.

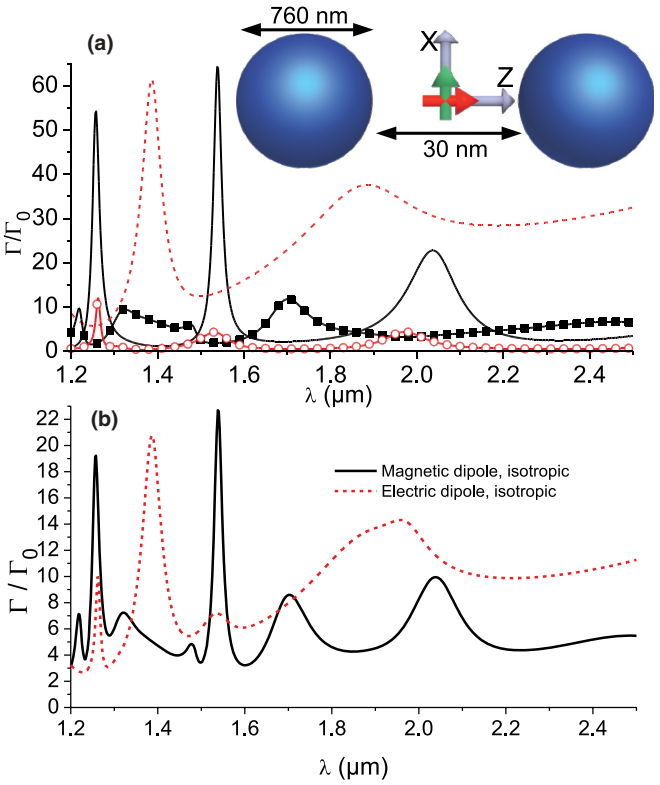

FIG. 5. (Color online) Normalized decay rates for a dimer of Si spheres, diameter 760 nm, nanogap length 30 nm, embedded in a dielectric background of refractive index $n = 1.45$. (a) Longitudinal coupling: (full black line) magnetic dipole, (dashed red line) electric dipole. Transverse coupling: (full black squares) magnetic dipole, (open red circles) electric dipole. Inset: sketch of the dimer configuration. The red and green arrows indicate the dipole orientation in longitudinal and transverse coupling, respectively. (b) Isotropic averages: (full black line) magnetic dipole, (dashed red line) electric dipole.

precisely to the decay rates calculated with the full GMM method (full black line). We remark that these expressions are valid either for a magnetic or an electric dipole emitter and are symmetric with respect to an interchange between α^u and α^v, which is equivalent to interchanging ϵ and μ in accordance with the conclusion of Ref. 20.

For the sake of completeness, we plot in Fig. 4 the calculated decay rate enhancements at $\lambda_0 = 1546$ nm when varying the distance between the dipolar emitter and the surface of the sphere for transverse and longitudinal couplings as well as for isotropically averaged dipole orientations. It is easy to observe that the maximum enhancement is always achieved for the smallest distance, as was expected from the above equations. At a very short distance (2 nm), the normalized decay rate of a magnetic emitter is enhanced by a factor 116 in longitudinal coupling and by a factor 52 when considering an isotropic average over all possible orientations, while the latter is limited to 12 for an electric dipolar emitter. When increasing the distance up to 50 nm, the decay rate enhancements decrease quasiexponentially (as illustrated by the straight lines in logarithmic scale), down to isotropic averages of 19 and 6.4 for the magnetic and electric dipole respectively.

IV. DIMER OF DIELECTRIC PARTICLES

Magnetic Mie resonances require a high index contrast that is not always compatible with experimental requirements. For lanthanide ions embedded in a solid environment like silica, the decrease of the refractive index contrast will spoil the magnetic response of the dielectric antenna. For such low refractive index contrasts, magnetic emissions can still be promoted for most dipole orientations by using a dielectric nanogap antenna, i.e., a dimer of spheres made of silicon, and by considering higher order multipolar resonances with higher quality factors. Figure 5(a) shows the radiative decay rate enhancements calculated using the GMM when a magnetic dipolar emitter is located in the center of a 30 nm nanogap separating two 760 nm diameter silicon spheres placed in a silica host ($n = 1.45$). In this configuration, the longitudinal magnetic dipole is resonant with the hexapoles of the particles ($N = 3$ in the GMM formalism) at $\lambda = 1.538$ μm. The normalized decay rate reaches a peak of 64.5 with a 24 nm linewidth (FWHM) for the magnetic emitter, while the electric emitter decay rate is enhanced by 14.6 (both values are taken in longitudinal coupling at $\lambda = 1.538$ μm). For a transverse coupling configuration, both electric and magnetic decay rates are weakly enhanced (4.19 for an electric dipole emitter and 1.91 for a magnetic dipole emitter at $\lambda = 1.538$ μm). The isotropic average over all possible dipole orientations displayed in Fig. 5(b) are 22.7 and 7.18 at $\lambda = 1.538$ for the magnetic and electric dipolar emitters respectively, which means that the magnetic deexcitation is promoted by a factor higher than 3 at this wavelength.

V. CONCLUSION

In conclusion, dielectric materials that support magnetic Mie resonances can efficiently tailor the magnetic local density of states and promote magnetic radiative decay in trivalent lanthanide ions. The conjunction of high quality factors and negligible ohmic losses allows the enhancement of magnetic emission while minimizing the competitive electric decay channels (both radiative and nonradiative). Using only four Mie coefficients, it is possible to analytically estimate the total and radiative decay rates of both electric and magnetic transition dipoles. The spectral widths of high-order Mie resonances in silicon spheres are well adapted to the narrow emission line of trivalent erbium ions at 1.54 μm, and a low refractive index contrast between the dielectric particle and the surrounding medium can be offset by using dimers of spheres with nanometer gaps. The lossless increase of the magnetic LDOS is thus highly efficient to tailor the symmetry of light emission and design microcavities for quantum electrodynamics and lasing.

ACKNOWLEDGMENTS

This research was funded by the French Agence Nationale de la Recherche under Contract No. ANR-11-BS10-002-02 TWINS.

*nicolas.bonod@fresnel.fr

[1]E. M. Purcell, Phys. Rev. **69**, 674 (1946).
[2]J. Gersten and A. Nitzan, J. Chem. Phys. **75**, 1139 (1981).
[3]R. Ruppin, J. Chem. Phys. **76**, 1681 (1982).
[4]P. Anger, P. Bharadwaj, and L. Novotny, Phys. Rev. Lett. **96**, 113002 (2006).
[5]S. Kuhn, U. Hakanson, L. Rogobete, and V. Sandoghdar, Phys. Rev. Lett. **97**, 017402 (2006).
[6]R. Carminati, J. J. Greffet, C. Henkel, and J. M. Vigoureux, Opt. Commun. **261**, 368 (2006).
[7]A. Kinkhabwala, Z. Yu, S. Fan, Y. Avlasevich, K. Mullen, and W. E. Moerner, Nat. Photonics **3**, 654 (2009).
[8]V. M. Shalaev, Nat. Photonics **1**, 41 (2007).
[9]M. Burresi, D. van Oosten, T. Kampfrath, H. Schoenmaker, R. Heideman, A. Leinse, and L. Kuipers, Science **326**, 550 (2009).
[10]T. Grosjean, M. Mivelle, F. I. Baida, G. W. Burr, and U. C. Fischer, Nano Lett. **11**, 1009 (2011).
[11]M. J. Weber, T. E. Varitimos, and B. H. Matsinger, Phys. Rev. B **8**, 47 (1973).
[12]Q. Thommen and P. Mandel, Opt. Lett. **31**, 1803 (2006).
[13]S. Karaveli and R. Zia, Opt. Lett. **35**, 3318 (2010).
[14]S. Karaveli and R. Zia, Phys. Rev. Lett. **106**, 193004 (2011).
[15]T. Feng, Y. Zhou, D. Liu, and J. Li, Opt. Lett. **36**, 2369 (2011).
[16]A. García-Etxarri, R. Gómez-Medina, L. S. Froufe-Pérez, C. López, L. Chantada, F. Scheffold, J. Aizpurua, M. Nieto-Vesperinas, and J. J. Sáenz, Opt. Express **19**, 4815 (2011).
[17]E. Palik and G. Ghosh, *Handbook of optical constants of solids* (Academic Press, Boston, 1998).
[18]B. Stout, A. Devilez, B. Rolly, and N. Bonod, J. Opt. Soc. Am. B **28**, 1213 (2011).
[19]B. Stout, J.-C. Auger, and J. Lafait, J. Mod. Opt. **49**, 2129 (2002).
[20]V. Klimov and V. Letokhov, Laser Physics **15**, 61 (2005).